

### Research on Engineering Structures & Materials



www.jresm.org



## Variable tube geometry micro channel heat exchanger (MCHX) using analytical and CFD analysis

Ram A, P D Jeya Kumar, Prince Arockia Doss

Online Publication Date: 30 January 2025

URL: <a href="http://www.jresm.org/archive/resm2025-472an1005rs.html">http://www.jresm.org/archive/resm2025-472an1005rs.html</a>

DOI: http://dx.doi.org/10.17515/resm2025-472an1005rs

Journal Abbreviation: Res. Eng. Struct. Mater.

#### To cite this article

Ram A, Kumar P D J, Doss P A. Variable tube geometry micro channel heat exchanger (MCHX) using analytical and CFD analysis. *Res. Eng. Struct. Mater.*, 2025; 11(5): 2231-2252.

#### Disclaimer

All the opinions and statements expressed in the papers are on the responsibility of author(s) and are not to be regarded as those of the journal of Research on Engineering Structures and Materials (RESM) organization or related parties. The publishers make no warranty, explicit or implied, or make any representation with respect to the contents of any article will be complete or accurate or up to date. The accuracy of any instructions, equations, or other information should be independently verified. The publisher and related parties shall not be liable for any loss, actions, claims, proceedings, demand or costs or damages whatsoever or howsoever caused arising directly or indirectly in connection with use of the information given in the journal or related means.



Published articles are freely available to users under the terms of Creative Commons Attribution - NonCommercial 4.0 International Public License, as currently displayed at here (the "CC BY - NC").



## Research on Engineering Structures & Materials



www.jresm.org

Research Article

# Variable tube geometry micro channel heat exchanger (MCHX) using analytical and CFD analysis

Ram Aa, P D Jeya Kumar \*,b, Prince Arockia Doss c

**Abstract** 

Dept. of Mechanical Eng., B.S. Abdur Rahman Crescent Institute of Science and Technology, India

#### **Article Info**

#### **Article History:**

Received 05 Oct 2024 Accepted 29 Jan 2025

#### **Keywords:**

Variable geometry; Calorie meter; Heat transfer coefficient; Analytical calculation; CFD The aim of this study is to improve condenser performance by incorporating unique tubes and shapes that control the volume of refrigerant. Analytical calculations were performed to determine hydraulic diameters for various tubes and port shapes. The heat and pressure drop across the condenser were estimated using the calculated hydraulic diameters. The refrigerant pressure drop correlation was chosen based on its advantages, and the findings were compared to experimental data (component calorimeter results). For the first time, two-phase density was calculated analytically, and its impact on heat transfer was investigated. The analytical results were compared to CFD simulation and experimental data. The findings demonstrated that an analytical method may be employed in the early stages of design during the development of automotive cooling units and that it could then be correlated with experimental data. This will eliminate the cost of developing prototype parts and shorten the lead time to market.

© 2025 MIM Research Group. All rights reserved.

#### 1. Introduction

A compact heat exchanger is a common piece of equipment used to effectively transfer heat between fluids. It is differentiated by laminar flow, small flow passageways, large heat transfer coefficients, and a high heat transfer area to volume ratio. The goal of compact heat exchangers is to reduce the size of the heat exchanger installation. They are designed to have a high area density, or a large area of heat transfer surface per heat exchanger volume. Plate and frame, plate-fin, spiral, ceramic, welded plate, brazed plate, and printed circuit are some examples of compact heat exchanger designs. Although there is little literature on the installation of small heat exchangers in the aluminium industry, efforts are being made to reduce installation sizes.

The heating, ventilation and air conditioning (HVAC) sectors have recently been interested in smaller heat exchangers, which are utilized in residential, commercial, and automobile air conditioning systems. The compact heat exchanger is a device used in air conditioner evaporators, car radiators & condensers, electronic cooling devices, charge air coolers, and cryogenic exchangers. Various enhanced surfaces have been created to increase heat transfer performance while reducing the size and weight of heat exchangers. Plain, wavy, offset, perforated, pin, and louvered fins are examples of common fin geometries. In a small automobile condenser, complicated geometries are often configured in a crossflow configuration with a louvered fin shape. Thermal resistance often dominates the airside of small heat exchangers, making about 80% of the overall thermal resistance, since the surface area for heat transfer on the air side is much bigger than the refrigerant side. Therefore, any enhancement in airside heat transfer enhances the heat exchanger's total performance. A thorough examination of how operating parameters affect airside pressure drop and heat transfer in MCHX under wet surface conditions was presented by Srisomba et al. [1]. The important variables affecting heat transfer performance were emphasized

\*Corresponding author: <a href="mailto:pdjeyakumar@crescent.education">pdjeyakumar@crescent.education</a>

°orcid.org/ 0000-0002-7358-0304; borcid.org/ 0000-0003-0298-9468; corcid.org/ 0009-0003-6833-3936

DOI: http://dx.doi.org/10.17515/resm2025-472an1005rs

Res. Eng. Struct. Mat. Vol. 11 Iss. 5 (2025) 2231-2252

and suggested correlations between pressure drop and heat transfer coefficient were presented. Kolepaka et al. [2] focused on comparing heat transfer rates between unidirectional parallel flow and bidirectional counterflow arrangements in heat exchangers. The study involved computational fluid dynamics (CFD) analysis and thermal analysis for various fluids (such as hot water, R134A, R22, and R600A) and different heat exchanger materials (aluminium and copper). The results indicate that counterflow exhibits higher heat transfer coefficients but lower heat transfer rates compared to parallel flow. Furthermore, the highest heat flux is achieved in a counterflow heat exchanger when using R600A as the refrigerant and copper as the material. Kabar et al. [3] studied a two-dimensional steady-state heat transfer problem in two parallel-plate microchannel heat sinks.

S. Singh and Kukreja [4] focused on the experimental calculation of the condensation heat transfer coefficient (HTC) in micro-fin tubes with different helix angles (15° and 18°). The experiments were carried out using refrigerant R-410A at various mass fluxes, vapor qualities, and saturation temperatures. The results show that the average heat transfer coefficients in micro-fin tubes were 1.15-1.47 times larger than those in smooth tubes. With an average variation of 5.71%, the generated correlation is in line with the experimental results. The results advance our knowledge and design of heat exchangers and offer important new insights on condensation heat transfer in micro fin tubes. Louver-directed flows, on the other hand, occurred when airflow is parallel to louvers at high Reynolds numbers.

The phenomenon was further validated by Achaichia and Cowell [5]. Chang and Wang [6] investigated and validated correlations for louvered fins using experimental results of heat transfer characteristics of various louver fin shapes. The parallel branching of R-134a and R-410A upward flow into mini-channel tubes from a circular header for the mass flux from 92 to 277 kg/m²s was studied by Kim and Bullard [7]. A parallel-flow heat exchanger with a two-pass configuration was the subject of an R-410A flow distribution study conducted by Kim [8]. For an input quality of 0.3 and a mass flux ranging from 50 kg/m²s to 70 kg/m²s, tubes were heated to maintain the test section outlet superheat at 5°C.

A Mathematical model for a parallel flow condenser that takes the dispersion of refrigerant flow was proposed by Liang et al. [9]. Investigations were conducted on the effects of aspect ratio, mass flow, and pass arrangement on pressure drop, heat transfer, and flow distribution. It has been discovered that altering the aspect ratio or pass arrangement has a greater impact on heat capacity than on pressure drop and flow distribution. Automotive heat exchangers were studied experimentally and through simulation, and a distributed parameter model was created and verified using coil designer software. According to research, condensers with shorter louvered fins may hold 3–8.6% more heat than those with longer fins [10]. To shorten the study time, numerical studies of the louvered fin array have been conducted extensively recently. A model based on finite volume was introduced by Panda et al. [11] to study microchannel heat exchangers with changeable tube and fin shapes. It was believed that the refrigerant flow into the tubes was distributed equally, and the suggested design's advantages included improved material usage and heat exchanger performance. These correlations did, however, significantly deviate from actual results because of disparate experimental and data reduction techniques.

This study's primary goal is to determine how various tube geometries affect pressure drop and heat rejection using analytical and computational fluid dynamics methods. According to reports, a number of improved surfaces were investigated to enhance air-side heat transfer capabilities while lowering the weight and size of the heat exchangers. These surfaces include simple, wavy, offset, perforated, pin, and louvered fins. Characterizing the frictional pressure loss in two-phase flow is an important factor to take into account when designing condenser/evaporator operations for air conditioning and refrigeration applications. As a first step, the two-phase density was determined analytically, and the consequences of heat transfer on the refrigerant side were investigated. With the increasing requirement to minimize the overall refrigerant charge in refrigeration systems, many heat exchanger tubes now have hydraulic diameters less than 1.2 mm. Despite this tendency, there has been little investigation on the modelling of two-phase pressure loss in micro-channels

of small diameters. As a result, this study intends to fill this gap by comparing research data to current correlations, which primarily apply to greater diameters (Di > 5 mm) and small tubes.

#### 2. Model of Automotive Condenser (Heat Exchanger)

The radiator where the gaseous refrigerant loses heat and transforms back into a liquid is called the air-conditioning condenser, and it is placed between the engine-cooling radiator and the car's grille. The interior is cooled by the liquid refrigerant as it passes through the dashboard's evaporator. An automotive condenser is constituted of tubes, inlet and outlet manifolds and fins. Partitions within the condenser's manifolds will guide the refrigerant flow along a predetermined direction. The overall contact surface area between the tube and the refrigerant increases when an efficient route arrangement is created. By giving the cooling medium (air) a wide surface area, the fins will assist heat to be forced into convection mode released from refrigerant through the connecting tubes. For the condenser to function, this heat rejection is essential. Fig. 1 depicts a condenser model.

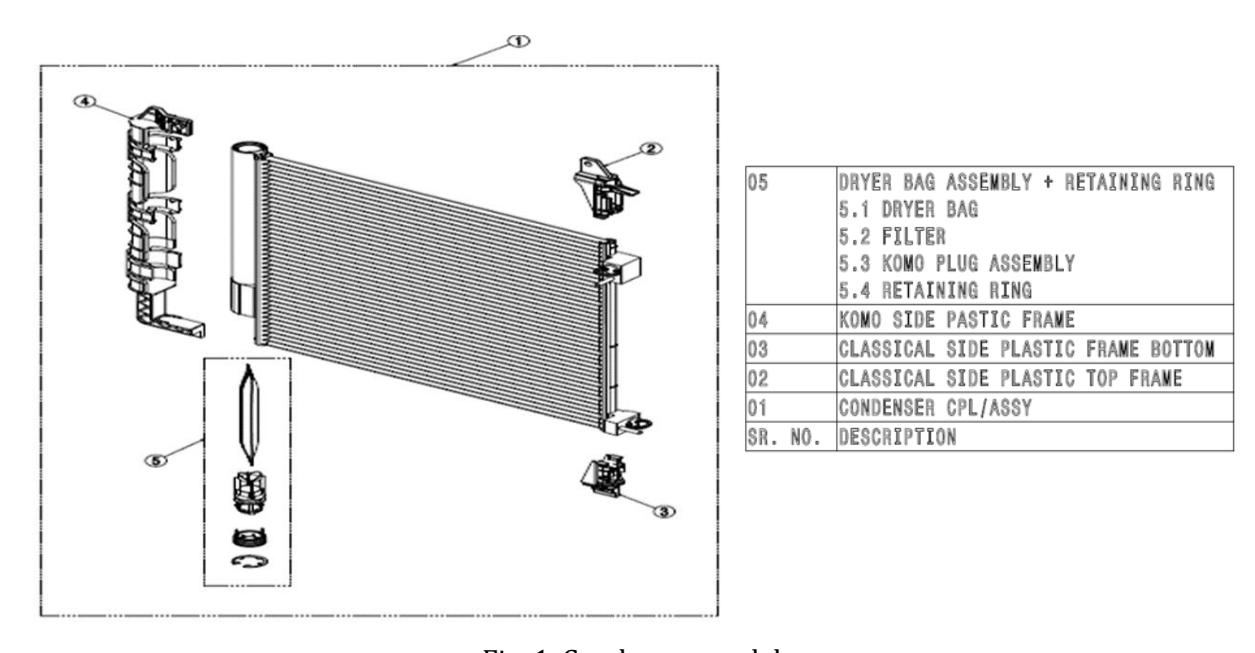
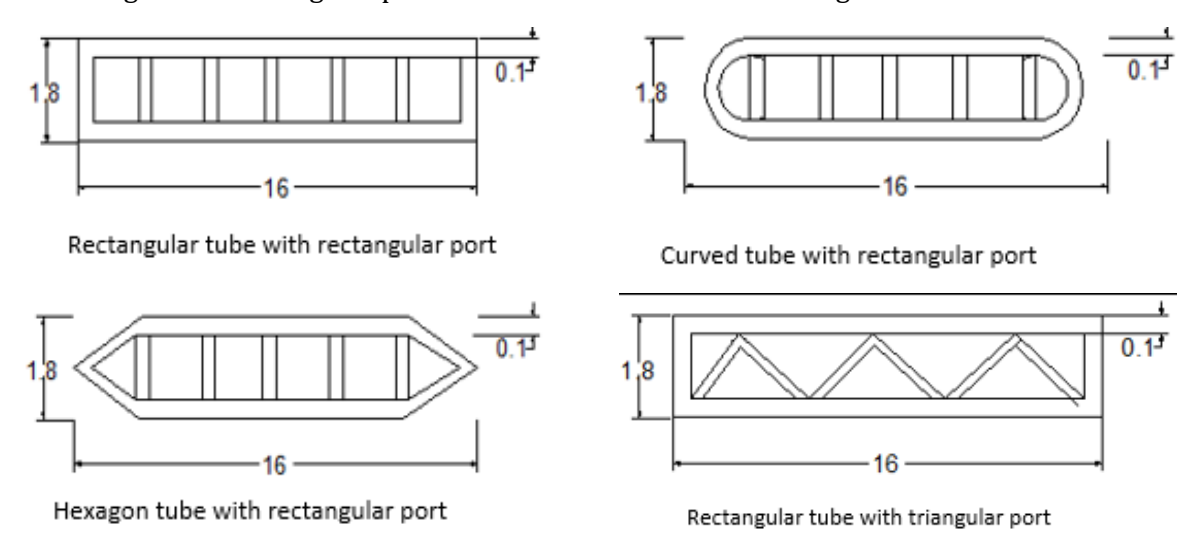


Fig. 1. Condenser model

#### 3. Tube Hydraulic Diameter Calculation

The geometrical sections of the tube considered in the study are oval, hexagonal, and rectangular, with rectangular and triangular ports for each section as shown in Fig. 2.



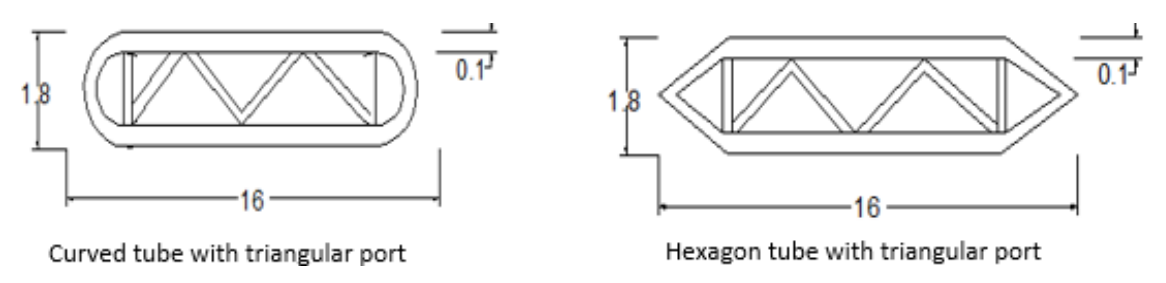


Fig. 2. Various Novel condenser tube and port shapes

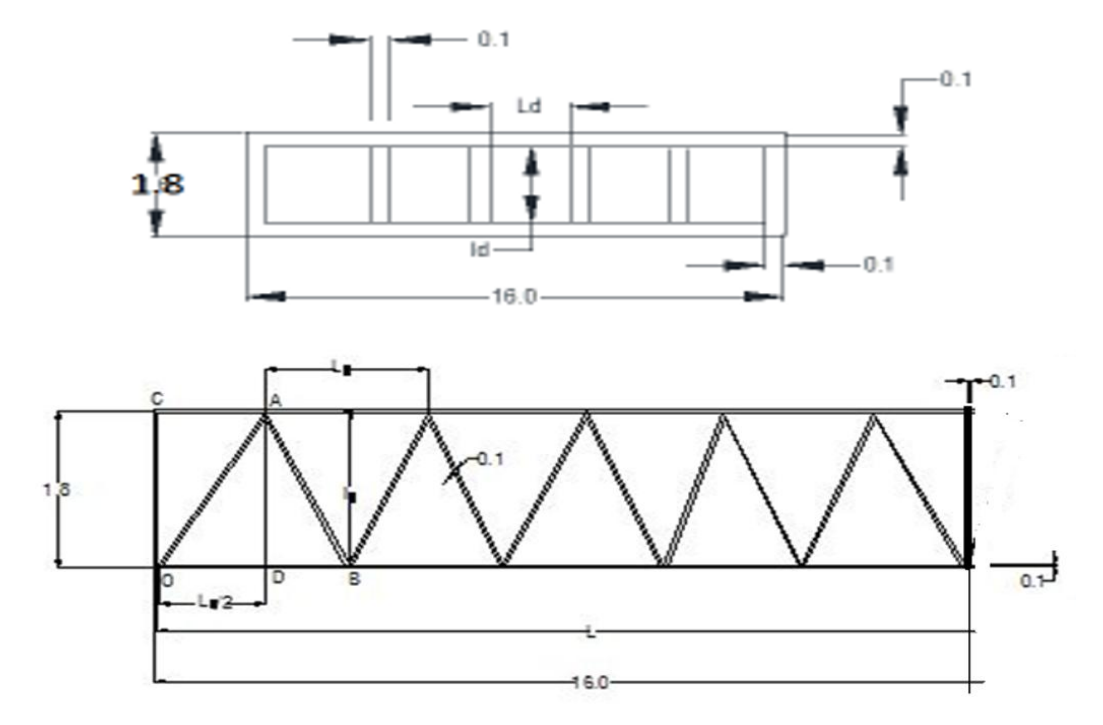


Fig. 3. Rectangular section with rectangular ports and triangular ports

Geometrical properties such as hydraulic diameter, aspect ratio, and perimeter are determined for the considered geometrical sections using mathematical techniques [12]. For evaporators, condensers, and heating and cooling coils under all operating conditions, a comprehensive general-purpose modelling tool for air/refrigerant heat exchangers has been created. Examples of Rectangular section with rectangular and triangular ports are shown in Fig. 3. As per Fig. 3,

- L = 15.8 mm (overall length in mm)
- $l_d = 1.5 \text{ mm}$  (height of the rectangle in mm)
- $l'_d = 1.8 \text{ mm}$  (outer height of the triangle in mm)
- $L_d$  = triangle base length in mm
- l = triangle side length in mm

$$r_d = \frac{L_d}{l_d} \tag{1}$$

#### Aspect ratio

- $\theta$  = Base angle of iso lateral triangle
- N = Total number of Triangle (except semi end triangle)

$$n = \frac{N}{2}$$
 = number of triangles in one side direction (2)

$$P_{w1} = \left(3 \times N / \tan \theta\right) \times \left(\frac{1}{\cos \theta} + 1\right) \tag{3}$$

$$P_{w2} = \left(\frac{L_d}{2} + l + l_d\right) \tag{4}$$

Perimeter of end triangle

$$P'_{w} = 1.5 \left[ \frac{2}{\tan \theta} \times \left( \frac{1}{\cos \theta} + 1 \right) \times (N+1) + 2 \right]$$
 (5)

 $P_w$ =Fluid flow surface area per unit length,  $D_h$  = hydraulic diameter

$$D_{h1} = \begin{pmatrix} 4 \times A / P_{w1} \end{pmatrix} \tag{6}$$

$$D_{h2} = \begin{pmatrix} 4 \times A / P_{w2} \end{pmatrix} \tag{7}$$

Where, A = Frontal Area of fluid flow passage in 'mm2

The expressions for aspect ratio & perimeter for variable geometry are derived based on the geometry and shape of the tube & ports. Based on these expressions, the hydraulic diameters for each tube shape were calculated [13]. The effects of the roughness parameters on heat transfer and friction characteristics were systematically investigated in a dimpled tube. The geometrical parameters are deduced from the basic dimensioning details from the tube geometry, the shape differences are captured using hydraulic diameter and the perimeters [6].

Table 1. Tube Hydraulic diameter for variable geometry

Sections	Aspect ratio (r <sub>d</sub> )	Perimeter P <sub>w</sub>	Hydraulic Diameter D <sub>h</sub>
	- a)	in mm	in mm
Rectangular tube with rectangular ports	$r_d = \frac{9.9375}{n} - 0.062$	$P_{w} = 3.2(1 + r_{d})$	$D_h = \frac{3.2 \times r_d}{\left(1 + r_d\right)}$
Hexagon tube with rectangular ports	$r_d = \frac{8.8125}{n} - 0.062$	$P_{_{\scriptscriptstyle W}}=3.2\big(1+\mathrm{r_{_{\rm d}}}\big)$	$D_h = \frac{3.2 \times r_d}{\left(1 + r_d\right)}$
Oval tube with rectangular ports	$r_d = \frac{8.8125}{n} - 0.062$	$P_{w} = 3.2(1 + r_{\rm d})$	$D_h = \frac{3.2 \times \mathrm{r_d}}{\left(1 + \mathrm{r_d}\right)}$
Rectangular tube with rectangular ports	$r_d = \left(\frac{2}{\tan \theta}\right)$	$P_{w1} = (3 \times N/\tan \theta) \times \left(\frac{1}{\cos \theta} + 1\right)$	$D_{h1} = \begin{pmatrix} 4 \times A / P_{w1} \end{pmatrix}$
Hexagon tube with rectangular ports	$r_d = \left(\frac{2}{\tan \alpha}\right)$	$P_{w} = \frac{3}{\tan \alpha} \left[ 1 + \frac{1}{\cos \alpha} \right]$	$D_{h} = \frac{4 \times A}{P_{w}}$
Oval tube with rectangular ports	$r_d = \left(\frac{2}{\tan \alpha}\right)$	$P_{w1} = 1.97485 + \frac{1.5}{\sin \alpha}$	$D_h = \left(\frac{4 \times A}{P_w}\right)$

#### 3.1 Two Phase Pressure Drop Correlations

As shown in equations 8, 9, and 10, a number of the two-phase pressure drop correlations are based on the separated flow model created by Lockhart and Martinelli (1949), Friedel (1979), and Chisholm (1967) [14, 15 and16]. Notably, the present study marks the first instance of conducting analytical calculations for two-phase refrigerant flow in micro-channels of this scale. The comparison of these correlations with the data obtained from the study will contribute to a more comprehensive understanding of two-phase pressure drop characteristics in small-diameter extruded aluminium micro-channels.

Lockhart Martinelli Correlation

$$\left(\frac{dp}{dz}\right) = \varphi_L \left(\frac{dp_F}{dz}\right)_L$$

$$\varphi_L = 1 + \frac{C}{X} + \frac{1}{X^2}, \varphi_G = 1 + CX + X^2$$
(8)

• Friedel Correlation

$$\left(\frac{dp}{dz}\right) = \varphi_{LO} \left(\frac{dp_F}{dz}\right)_{LO}$$

$$\varphi_{LO} = E + \frac{3.24 \times F \times H}{Fr^{0.045} \times we^{0.035}}$$
(9)

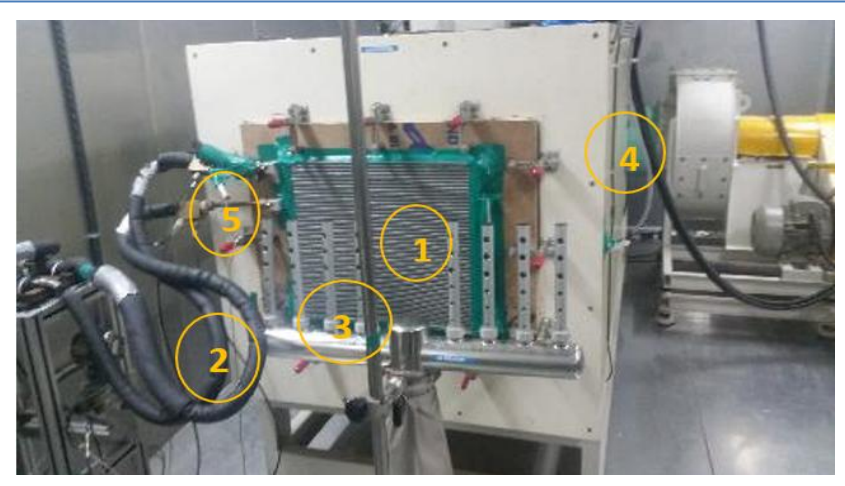
• Chisholm Correlation

$$\left(\frac{dp}{dz}\right) = \varphi_{LO}\left(\frac{dp_F}{dz}\right)_{LO} 
\varphi_L = 1 + (Y^2 - 1) * \left\{Bx^{\frac{(2-n)}{n}}(1-x)^{\frac{(2-n)}{2}} + x^{2-n}\right\}$$
(10)

In a related study by Liang Ye, Ming Wei Tong, and Xin Zeng [17], the heat transfer performances of parallel flow (PF) and multi-parallel pass condensers were investigated at air velocities of 2.5 m/s and 4.5 m/s. The results clearly indicate that the overall heat transfer of the Multi Parallel Pass (MPP) condenser exhibited a higher performance, surpassing the parallel flow condenser by 10% for an automotive application. These findings underscore the potential advantages of the multi-parallel pass configuration in enhancing heat transfer efficiency in the context of automotive condenser applications. In another study [18], a visualization experiment has been carried out to study the effect of the header and channels' orientations on the phase distribution of two-phase flow in three parallel micro-channels. The pressure drops properties of R134a within multiport micro-channels on several refrigerants, including R236ea (low pressure) and R410A, have been experimentally studied [19].

### 4. Experimental and Analytical Results

The experiment involved the base configuration of an oval tube shape with a rectangular port in the condenser calorimeter, as depicted in Figure 4. The test rig is designed for assessing the performance of a heat exchanger. The setup includes provisions for supplying high-pressure air to the cold side of the test unit, consisting of a blower, dampers, and necessary instruments. The test rig also incorporates a water inlet system, with refrigerant supplied through the tube (hot) side of the test unit. During the experiments, the mass flow rate of the refrigerant was adjusted using a flow control valve, ranging from 3 to 7 kg per minute (kg/m). Simultaneously, the air velocity is controlled by adjusting the damper position, ranging from 2 to 10 meters per second (m/s). Measurements of refrigerant outlet temperature, air inlet and outlet temperatures, and pressure drops across the air and sides of the refrigerant are recorded for different mass flow rates. Based on these measurements, the performance of the heat exchanger is estimated, and results are plotted graphically.



- [1]Condenser
- [2] Refrigerant Pipe
- [3] Air flow sensors
- [4]Wind duct
- [5] Refrigerant sensor

Fig. 4. Experimental setup of condenser calorimeter

The temperature measurements of the air-steam mixture are conducted using T-type thermocouple meshes inserted from the top and bottom surfaces of the test section. These meshes consist of multiple thermocouples with an average span-wise interval of 40 mm. Air velocity is measured with a portable anemometer, and the air pressure drop across the heat exchanger is measured using calibrated pressure transducers. The setup also includes pre-calibrated thermocouples to measure refrigerant, inlet, and outlet temperatures, as well as a flow meter to measure the refrigerant volume flow rate. Data acquisition is facilitated through a data acquisition system. To minimize heat loss, all components and pipes are insulated with a 10 mm thick glass wool layer. The experimental setup enables comprehensive data collection, allowing for accurate evaluation and analysis of the heat exchanger's performance.

#### 5. Uncertainty Analysis

Uncertainty in experimental results is inevitable due to various factors such as instrument precision, environmental influences, and measurement methods. Identifying and quantifying these uncertainties helps in assessing the reliability of the findings.

- Thermocouple has a certain degree of accuracy (±1°C, for example), which affects temperature measurements on both the air and refrigerant sides.
- Refrigerant flow rate measurement depends on the flow meter's accuracy.
- Ambient temperature fluctuations can slightly affect the heat loss or gain, despite the insulation, thus impacting measured temperatures.
- If thermocouples aren't precisely positioned, it can lead to spatial inaccuracies.
- The accuracy of the air velocity measurement depends on how well-calibrated the anemometer is.

The overall uncertainty is influenced by the variability between several experimental runs (repeatability) and possible variations when the experiment is repeated using different setups or operators (reproducibility), particularly if specific conditions or adjustments cannot be replicated exactly each time. Test carried out at an authorized component calorimeter lab in Germany with a high reliability level of the data output. Table 2 displays the experimental findings for the samples with an average input pressure of 16.2 bar (abs), superheat temperature of 25 °C, sub cool temperature of 5 °C, and air temperature of 35 °C. The experimental data was collected using a component calorimeter, and the corresponding results are presented graphically in Figure 5. This experimental setup allowed for the measurement and analysis of specific performance parameters or characteristics, and the graphical representation in Figure 5 serves as a visual depiction of the outcomes derived from the experimentation in the component calorimeter.

Table 2. Experimental results showing multiple samples

Air velocity (m/s)	Parameter	Sample 1	Sample 2	Sample 3	Sample Average
	Average Heat Rejection kW	20.81	21.37	21.18	21.12
	Air velocity m/s	7.98	7.99	7.99	7.98
	Airside pressure Drop Pa	344.60	350.74	350.68	348.67
0	Average Pressure bar	15.94	15.9	16.03	15.96
8	Refrigerant side Pressure Drop mbar	2405.75	2352.58	2465.79	2408.04
	Refrigerant Mass flow kg/min	6.71	6.85	6.82	6.79
	Average Heat Rejection kW	17.56	17.79	17.68	17.67
	Air velocity m/s	5.04	5.05	5.02	5.04
	Airside pressure Drop Pa	167.14	169.64	168.4	168.39
	Average Pressure bar	16.31	16.32	16.32	16.32
5	Refrigerant side Pressure Drop mbar	1877.68	1757.96	1921.08	1852.24
	Refrigerant Mass flow kg/min	5.77	5.81	5.79	5.79
	Average Heat Rejection kW	9.72	9.84	9.67	9.74
	Air velocity m/s	2.05	2.03	2.03	2.03
	Airside pressure Drop Pa	41.32	40.84	41.22	41.13
	Average Pressure bar	16.25	16.28	16.29	16.27
2	Refrigerant side Pressure Drop mbar	682.29	657.34	655.89	665.18
	Refrigerant Mass flow kg/min	3.23	3.27	3.21	3.24

Fig. 6 compares experimental and Friedel correlation results, demonstrating good agreement. This suggests the Friedel correlation accurately predicts the phenomenon under study, indicating its usefulness in understanding and predicting system behavior. Additionally, the pressure drop through the condenser for oval-shaped tubes is calculated using these correlations in an analytical technique, and the results correlate with the analytical method as seen in Figures 6, 7, and 8. The results obtained from the Lockhart Martinelli correlations show slight deviations when compared to the experimental results. The Chisholm correlation results exhibit greater deviations in comparison to the experimental results as well as the results obtained from the Friedel and Lockhart Martinelli correlations.

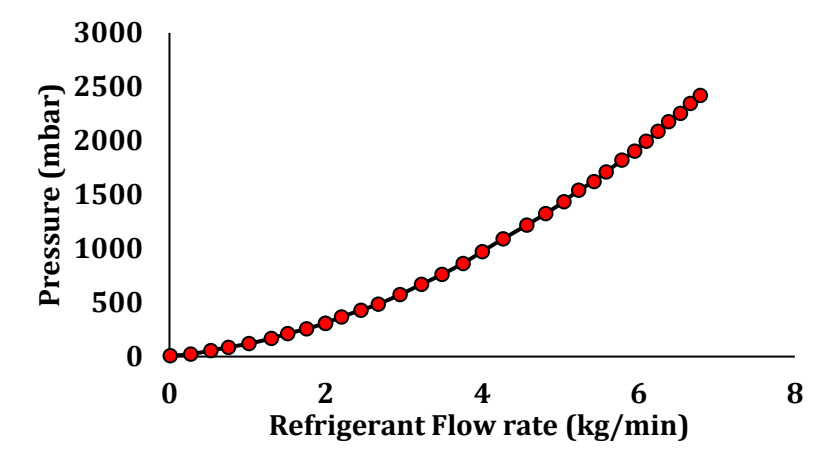


Fig. 5. Experimental refrigerant side pressure drop

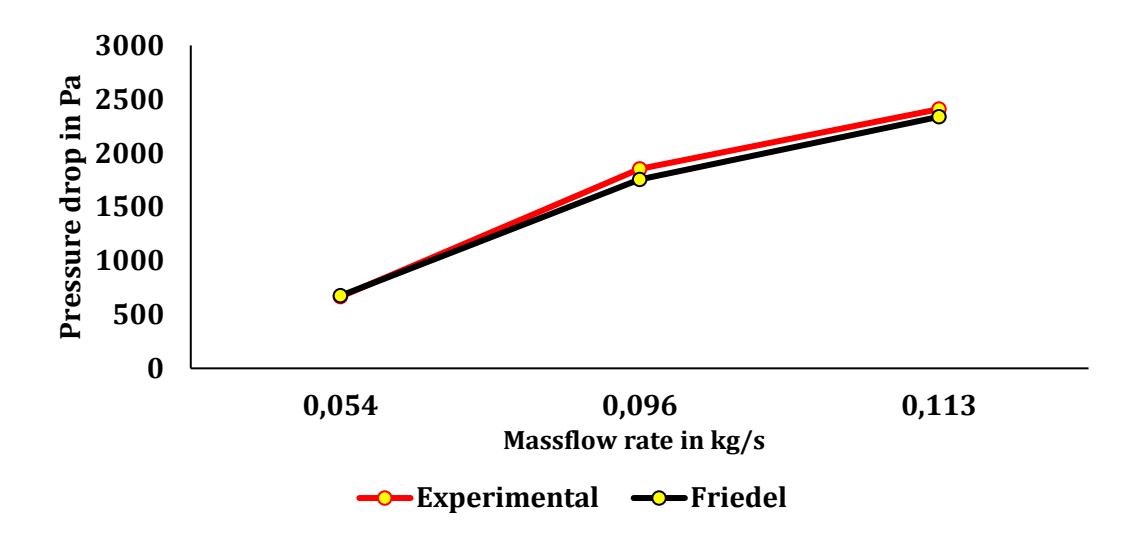


Fig. 6. Friedel correlation vs Experimental

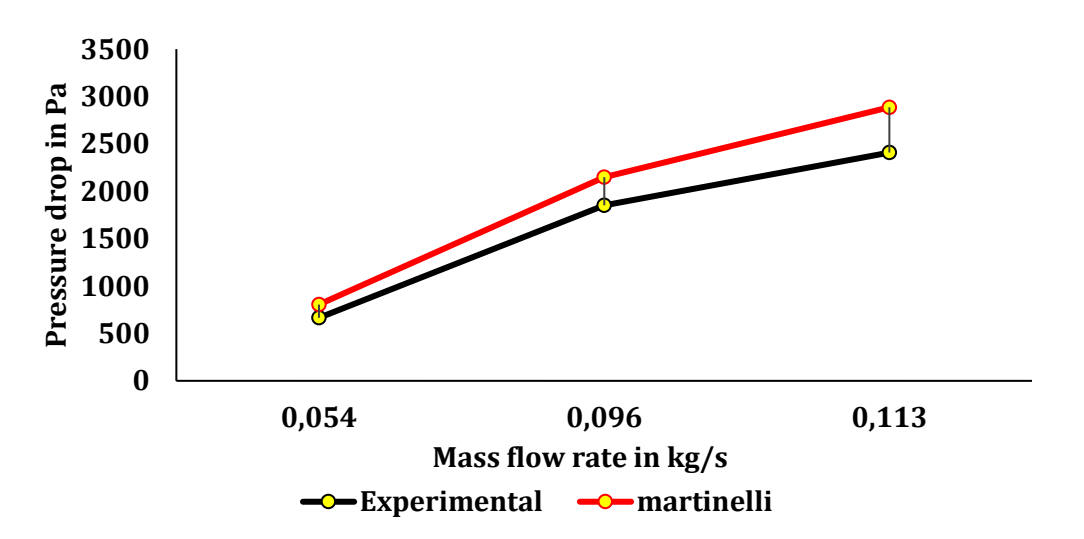


Fig. 7. Experimental vs Lockhart Martinelli

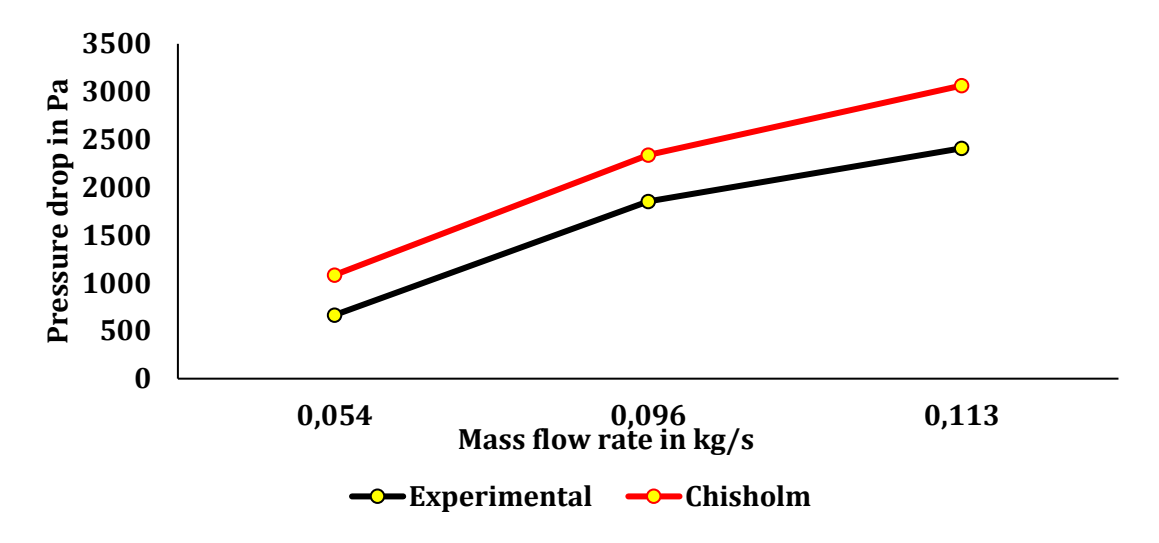


Fig. 8. Experimental vs Chisholm correlation

Table 3. Pressure drops between Analytical data and Experimental data

Ref.	Pressure Drop in mbar (Oval-Rec Section)- Correlations						
Mass flow rate	Friedel	Lockhart & Martinelli	Chisholm	Experimental			
kg/s	rrieuei	Lockilai t & Mai tillelli	Cilisilollii	Result			
0.054	708	855	1140	665			
0.096	1842	2282	2464	1852			
0.113	2455	3063	3227	2408			

Table 3 shows the pressure drop of the Friedel correlation for different refrigerant flow rates (kg/s) that were closer to the experimental results of pressure drop. So, the Friedel correlation was considered for the analytical calculation for different tube and port shapes.

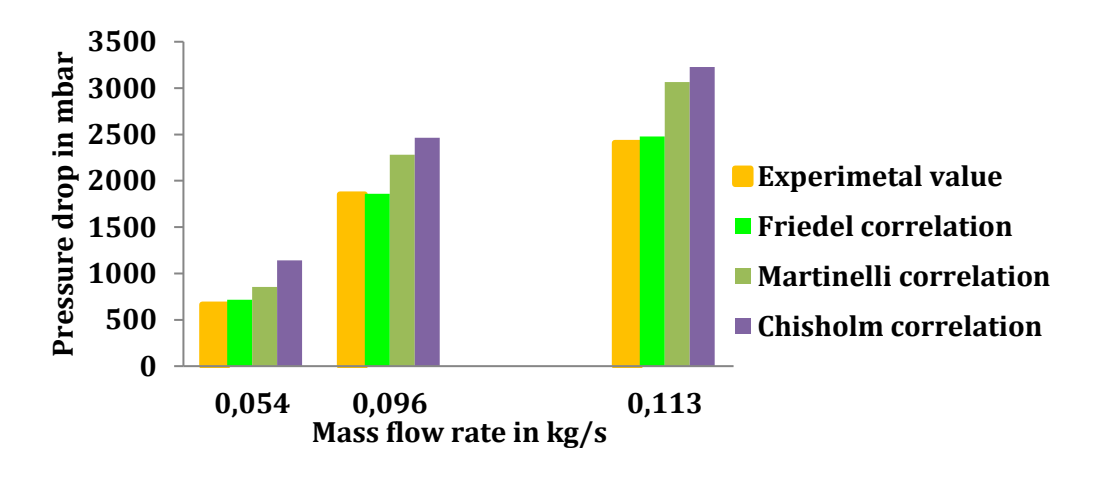


Fig. 9. Summary of correlation data vs Experimental Data

Table 4. Analytical results of variable geometry Pressure drop (Refrigerant side)

Ref.	Pressure Drop in mbar using Friedel Correlations						
Mass flow rate kg/s	Rec-Rec	Oval-Rec	Hex-Rec	Rec-tri	Oval-tri	Hex-tri	
0.054	674	708	774	832	920	1207	
0.096	1753	1 842	2015	2164	2394	4421	
0.113	2337	2455	2685	2885	3190	5889	

The results show that the refrigerant pressure drop for the rectangular port was lesser compared to other tubes and port shapes. Later, with the help of refrigerant pressure drop, the heat rejection for various tube & port shapes was calculated as shown in Table 5. The results show that the tube with a hexagon shape has a better heat transfer coefficient, but the refrigerant side pressure drop is very high.

Table 5. Analytical results of variable geometry Heat transfer co-efficient (Refrigerant side)

Refrigerant Side Heat Transfer Co-efficient (W/m <sup>2K</sup> )								
Refrigerant Mass flow rate (Kg/s)	Rec-Rec	Oval-Rec	Hex-Rec	Rec-tri	Oval-tri	Hex-tri		
0.054	2330	2345	2418	2405	2494	3024		
0.096	3605	3611	3723	3701	3840	4269		
0.113	4102	4118	4246	4221	4379	4869		

Further, CFD analysis was made to understand the behavior of heat transfer coefficient and pressure drop for different tube shapes. Using the obtained theoretical correlations, the pressure drops and heat transfer coefficient for various geometrical shapes at different flow rate conditions are calculated. These obtained results are compared with the numerical results. The chosen rectangular tube with rectangular ports as a benchmark analytical result is compared with experimental and numerical results. With the same agreement, analytical and numerical results for the other cases are also compared. The numerical results of heat rejection on the refrigerant side are compared with the experimental results as shown in Table 6. The lesser error percentage revealed that there is good agreement between the analytical and experimental values of heat rejection.

Table 6. Comparison between anal	lytical and experimental	Heat rejection	(Refrigerant side)
Tuble of domparison between and	i y cicai ana capei imena	i iicat i cjectioii	( Iteli igei alle blac)

Mass flow rate kg/s	Inlet temp °C	Inlet Enthalpy kJ/kg	Out Temp °C	outlet Enthalpy kJ/kg	Heat rejection (analytical) kJ	Heat rejection (experimental) kJ
0.054	83	460	43	260	10.8	9.72
0.096	83	460	44	262.43	18.9	17.56
0.113	83	460	49	270.07	21.4	20.81

#### 6. CFD Simulation

The numerical approach is the best approach to analyse the two-phase flow behaviour of the refrigerant as a full-scale model. Bensafi, Borg, and Parent [20] studied the computational model of detail design of plate & fin tube heat exchangers for various refrigerant mixtures of R32, R1, 25 & R134a. Ansys-Fluent utilizes a finite volume approach to simulate fluid flow, employing a RANS kepsilon model. The volume fraction represents the occupied space of each phase in the simulation domain, assuming that each cell is filled with one phase and not empty or a vacuum. The conservation equations for mass and momentum are applied separately to each phase. Heat transfer and energy equations are not considered in this model, and there is no phase change or interphase mass and momentum transfer. The interaction between phases requires additional closure models such as Interaction Length Scale, Interaction Area Density, Drag & Lift Force, etc. These models and parameters are essential for capturing the forces exerted by the phases on each other. Through a detailed examination of heat conduction in solids and a transient 1D analysis, a numerical model [21] of the fluid dynamic and thermal behaviour of condensers and evaporators has been created. The conservation equations (momentum, continuity, energy, and vapor species) are given in Equations 11, 12, 13, and 14, respectively.

• Momentum equation:

$$V_{p} \frac{\partial \overline{\rho v}}{\partial t} + \dot{m}_{g,e^{s}} v_{g,e^{s}} + \dot{m}_{1,e^{s}} v_{1,e^{s}} - \dot{m}_{g,w^{s}} v_{g,w^{s}} + \dot{m}_{1,w^{s}} v_{1,w} = (p_{P} - p_{E})A - \bar{\tau}_{w} P \Delta z - mg \sin \theta \qquad (11)$$

• Continuity equation:

$$V_p \frac{\partial \overline{\rho_p}}{\partial t} + m_e - m_w = 0 \tag{12}$$

• Energy equation:

$$\frac{\partial \check{\rho}_P \bar{e}_P}{\partial t} A \Delta z + \dot{m}_P^S e_e - \dot{m}_W^S e_W = \bar{q}_P P \Delta z + \frac{\partial \bar{P}_P}{\partial t} A \Delta z \tag{13}$$

• Vapor species equation:

$$\frac{\partial(\rho\omega_v)}{\partial t} + \nabla(\rho\omega_v\overline{w}) = \nabla(\rho D_e\overline{V}\omega_v) + S_v = 0 \tag{14}$$

The distribution is greatly impacted by the pressure drop that occurs during phase shift in the microchannel tubes used in the suggested system. User-defined functions are to estimate the pressure decrease. Heat transfer models are not used, and associated characteristics are not simulated, despite the fact that heat transfer for phase change within the tubes and consequently influences the pressure drop. Rather, the user-defined pressure drops calculations assume heat flux value as constant for heat transmission in the tubes. For the single- and two-phase superheated areas, different equations are used to calculate the pressure decrease. The tube's intake condition and the percentage of the tube that is occupied by the two-phase region—known as the Length Ratio (LR) and calculated—determine the pressure drop. The Blasius correlation and the Darcy-Weisbach equation are applied to single-phase pressure decrease. A homogeneous formulation with the Smoothed Muller-Steinhagen & Heck friction factor correlation is used to compute the pressure drop for two phase flows. The formulation treats both phases as a homogeneous mixture, though they were one phase with identical velocities. Assuming a homogeneous two-phase mixture, density and viscosity are computed using the Reynolds number. Fig. 10 shows the computational domain.

#### **6.1 Input Parameters for Simulation**

There is very little variation in the data above 3 million, which is thought to be the ideal mesh count for this inquiry. Reference pressure is taken as 2408 mbar from the experimental results. A hybrid mesh (hex-dominated mesh) of base mesh size of 1.2 mm with 5 layers is chosen for the simulation. Based on the standard correlation, results are calculated as a rough estimation, and at the same time, numerical results are helped to validate the geometry optimization in an accurate manner. Initially the experimental results are validated with the numerical result; based on this numerical result accuracy, further geometry optimization study was made.

• Refrigerant Properties

 $\begin{array}{lll} \text{Specific heat (Cp)} & :1.1604 \text{ kJ/kgK} \\ \text{Thermal Conductivity (k)} & :0.0182 \text{ W/mK} \\ \text{Absolute Viscosity (P)} & :1.411e-5 \text{ kg/ms} \\ \text{Density ($\rho$)} & :69.589 \text{ kg/m}^3 \end{array}$ 

• Aluminium material Properties

 $\begin{array}{ll} \text{Density ($\rho$)} & :2719 \text{ kg/m}^3 \\ \text{Specific heat (Cp)} & :0.871 \text{ kJ/kg K} \\ \text{Thermal Conductivity (k)} & :202.4 \text{ W/mK} \end{array}$ 

Normally, analytical study is preferred to compare the experimental results with a moderate accuracy level. For high accuracy and for complex shape & visualization, numerical results are employed. In the numerical analysis of two-phase flow behaviour within the heat exchanger, certain assumptions are typically made to simplify the complex flow and heat transfer dynamics. Those are,

- Flow is often assumed to be steady, meaning that variables like pressure, temperature, and velocity do not change with time. However, the real systems experience transient behaviour, especially during startup or shutdown, so assuming steady-state can overlook fluctuations in temperature and flow rate.
- Flow and temperature across the tube cross-section or at inlets are assumed to be uniform; however, in reality, flow and temperature profiles vary across the tube diameter, especially due to boundary layer development and turbulence.
- Gravitational forces and buoyancy effects are often ignored, especially in horizontal or small-scale models, assuming they have minimal impact.
- Two-phase flow analysis often simplifies phase transitions, assuming smooth transitions between liquid and vapor phases or using an idealized model.

Table 7. Boundary condition for CFD simulation

Refrigerant Inlet Temp	Tr,i	83.4 °C
Refrigerant Pressure	Pr,i	16.2 bar
Mass Flow rate	mref	0.054 kg/s
Air Inlet Temp	Ta,i	35 °C
Convective heat transfer coefficient	(h)	$325 \text{ w/m}^2\text{K}$

The input boundary conditions are specified in Table 7; the mass flow inlet is maintained as constant at the inlet, and pressure outlet boundary conditions are used as outlet boundary conditions. Convective heat transfer coefficient used as a constant wall boundary on the tube outer surface. The surrounding conditions are maintained as atmospheric conditions (35 °C and 1 ATM). The boundary condition for the condenser was considered for the CFD simulation as shown in Fig. 11. The cross section of various tubes was analysed in CFD to understand the temperature and pressure contours across the length for different pass structures.

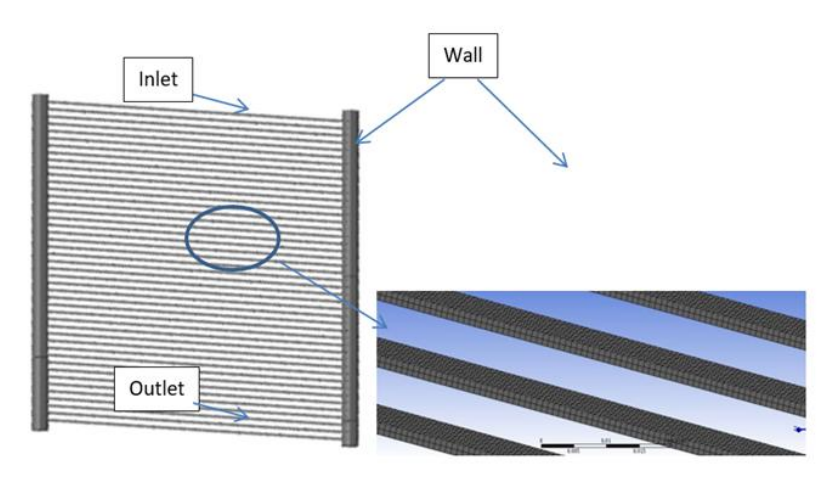


Fig. 10. Computational Domains

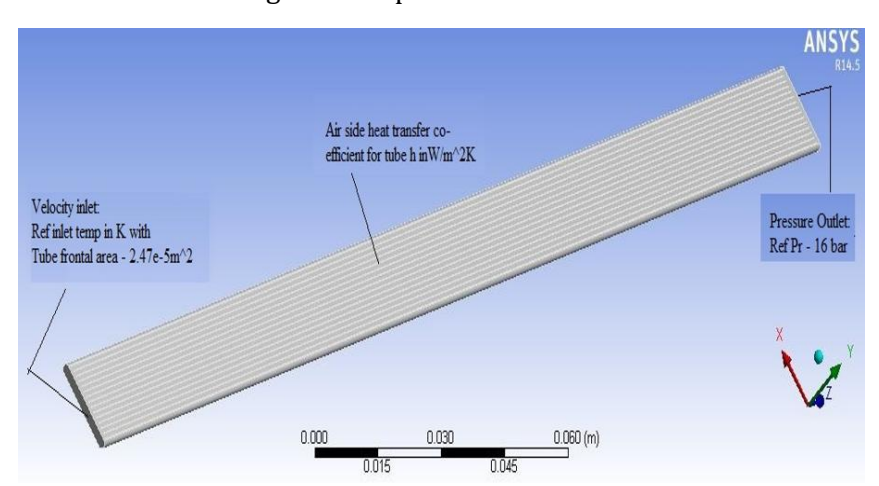


Fig. 11. Boundary condition used in oval shape tube

Numerical analysis of the two-phase refrigerant flow is the best approach to analyse the two-phase flow behaviour of the refrigerant; ANSYS-Fluent is used as a numerical solver. Figs. 12 & 13 show the temperature contour for the oval-shaped tube varies from pass-1 to pass-4, and the temperature drops from 74°C to 48°C at the outlet of the condenser, respectively. Due to the flow of the refrigerant, the heat to the atmosphere is rejected. Full model simulation was carried out to understand the behaviour of two-phase flow in refrigerant tubes in contact with the frontal airflow, which rejects the heat into the atmosphere. The heat is absorbed by the evaporator due to cabin heat load to attain the thermal equilibrium.

Table 8. Mesh independent study

Mesh Count in (million)	Pressure Drop mbar	Result Variation in %
1.5	2650	9.2
2.0	2580	6.67
2.5	2523	4.78
3.0	2494	3.57
3.5	2491	3.46

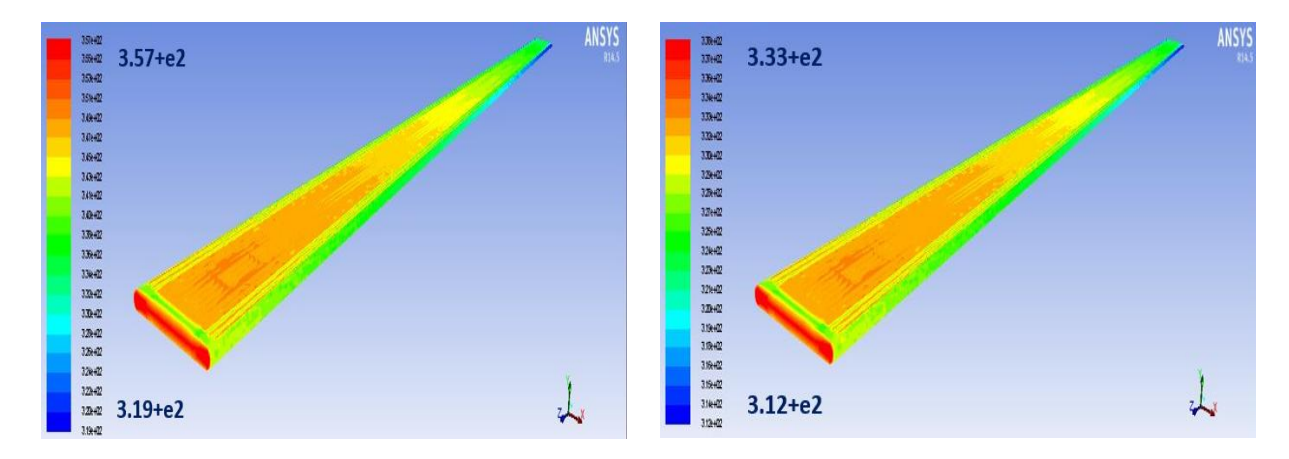


Fig. 12. CFD simulation of pass 1 and 2

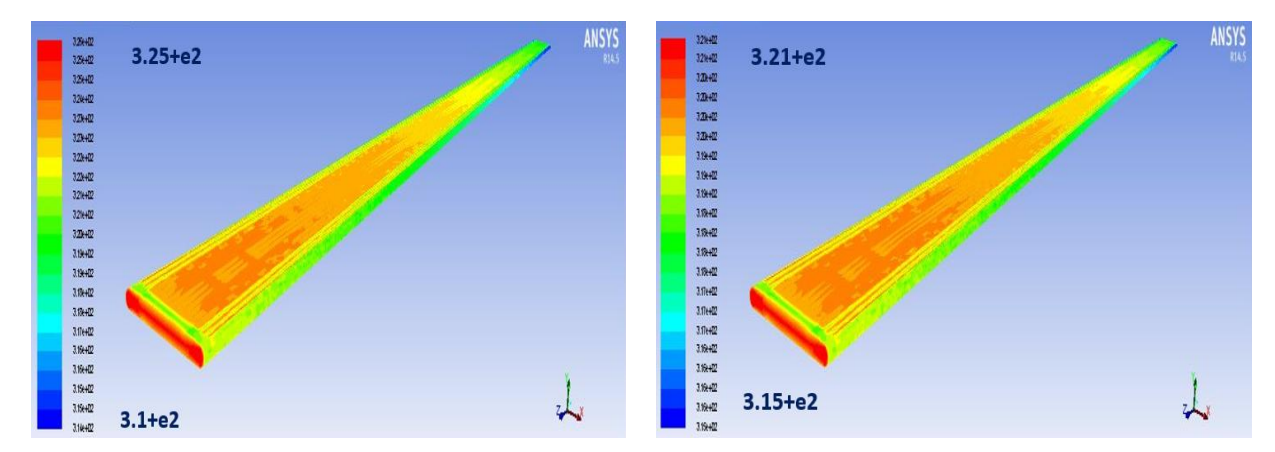


Fig. 13. CFD simulation of pass 3 and 4

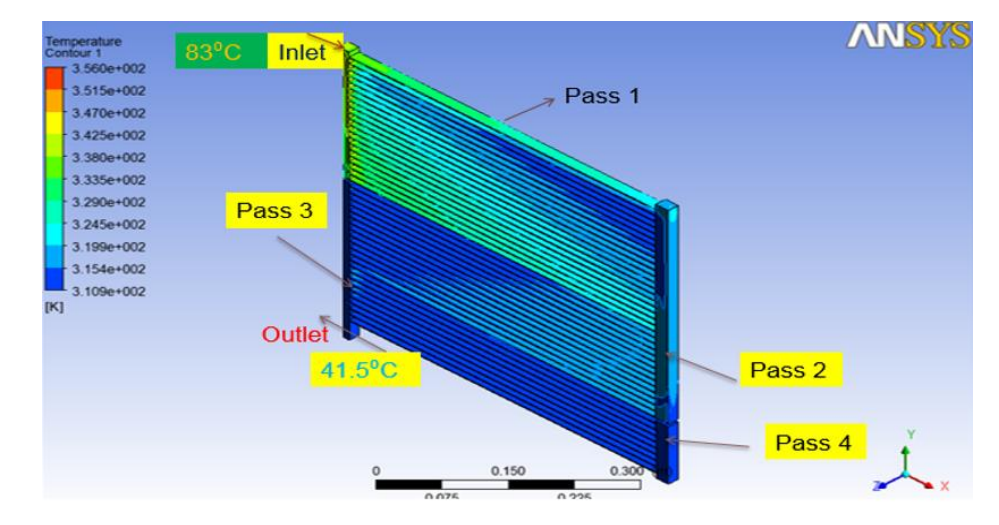


Fig. 14. CFD of condenser model with temperature contour

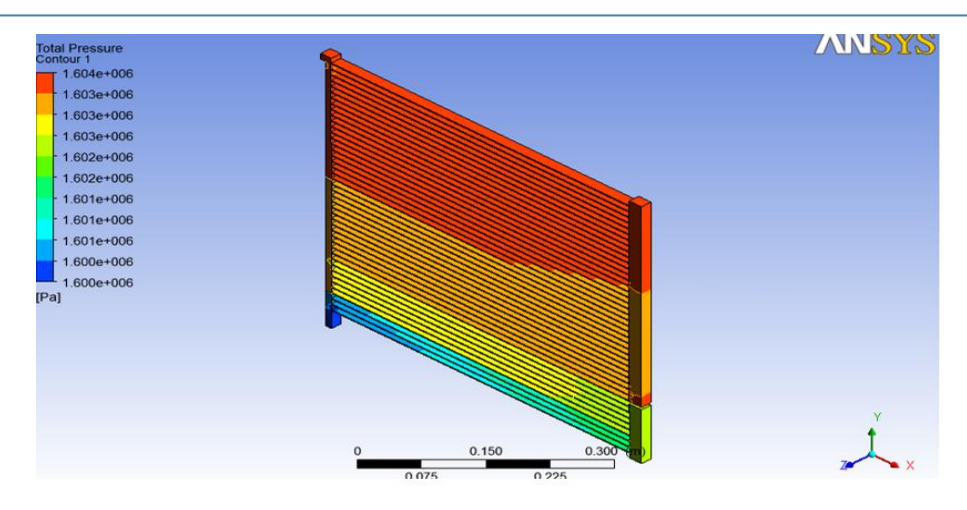


Fig. 15. CFD of condenser model with pressure contour

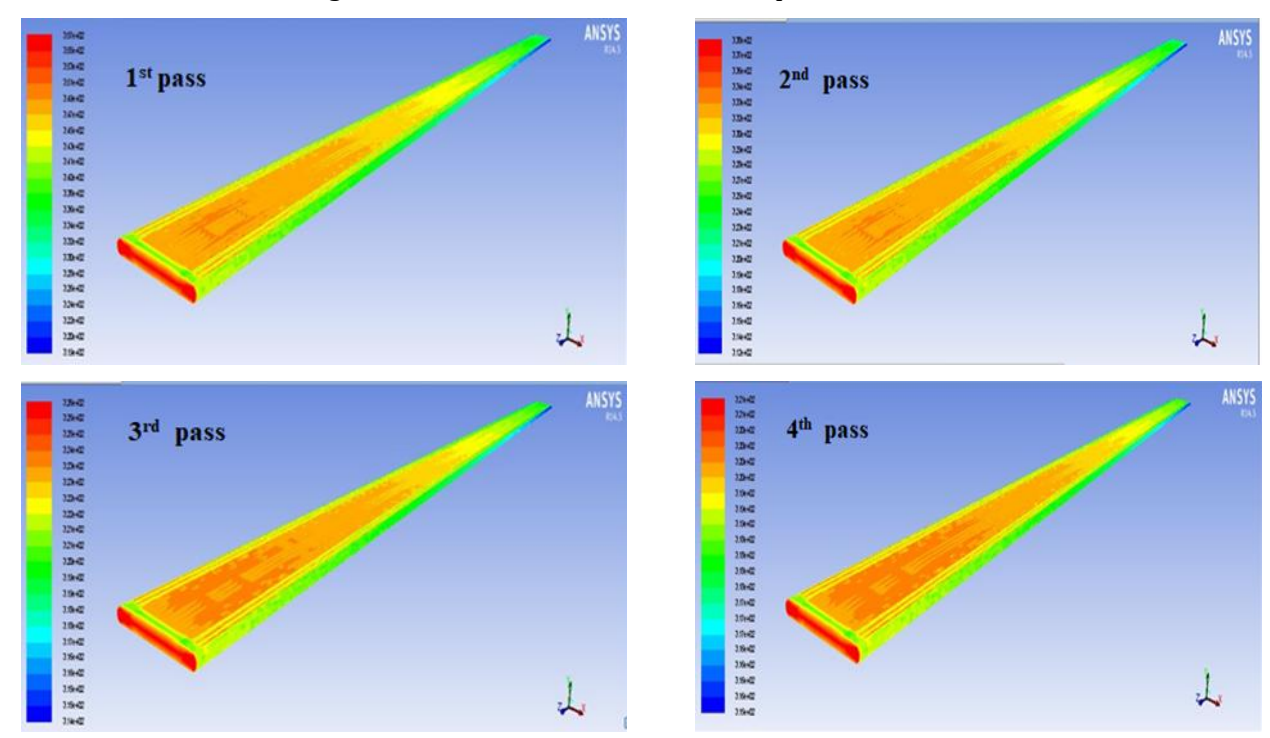
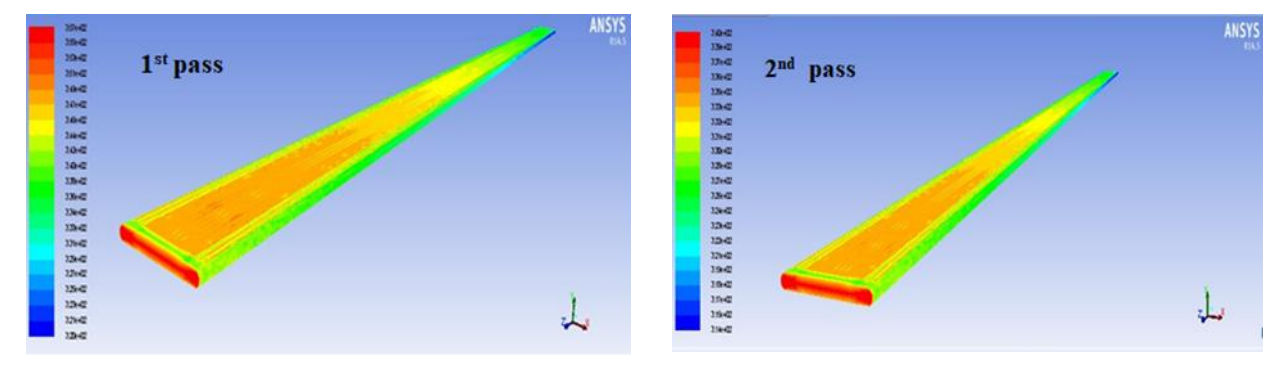


Fig. 16. Oval tube temperature contour at 2 m/s



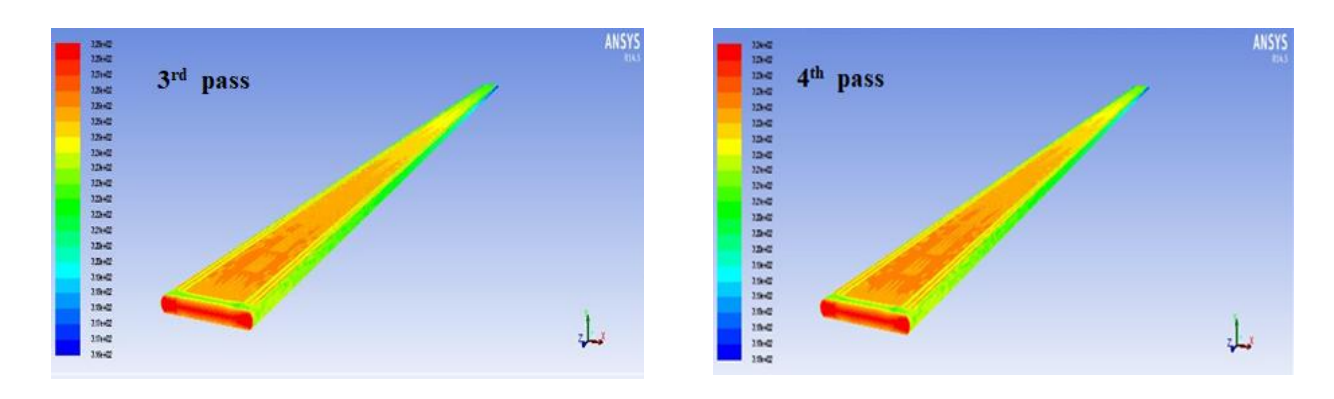


Fig. 17. Oval tube temperature contour at 5 m/s

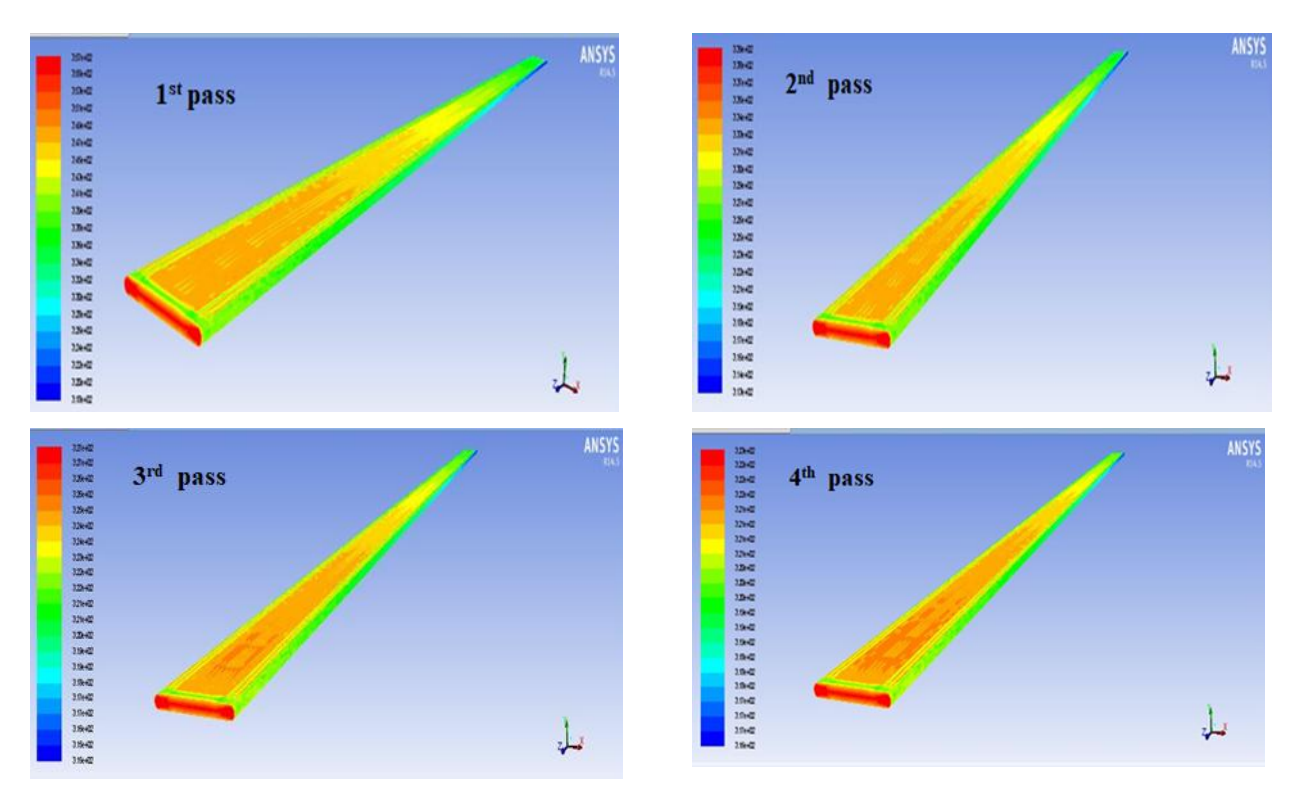
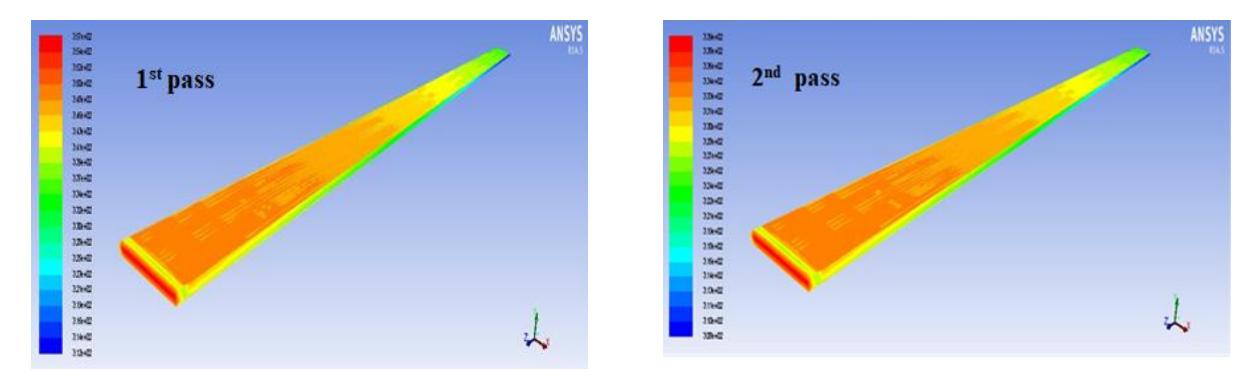


Fig. 18. Oval tube temperature contour at 8 m/s



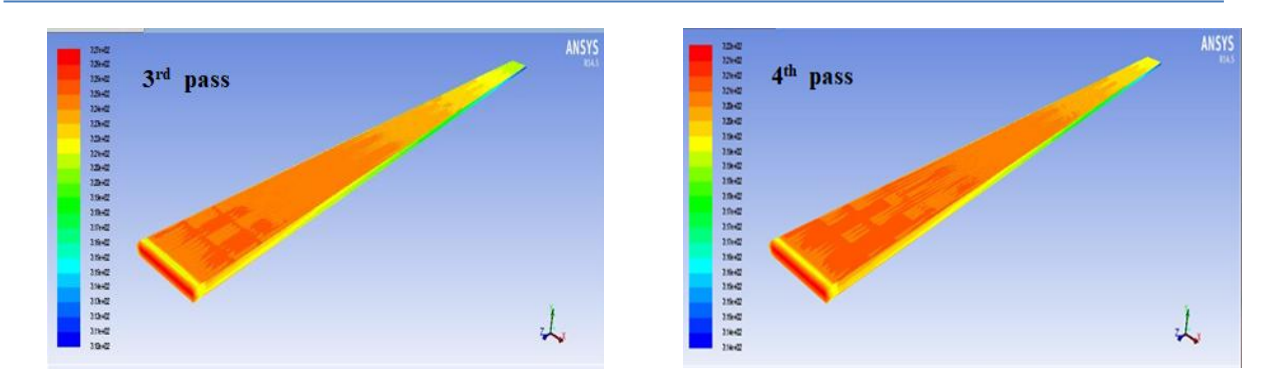


Fig. 19. Hexa tube temperature contour at 2 m/s

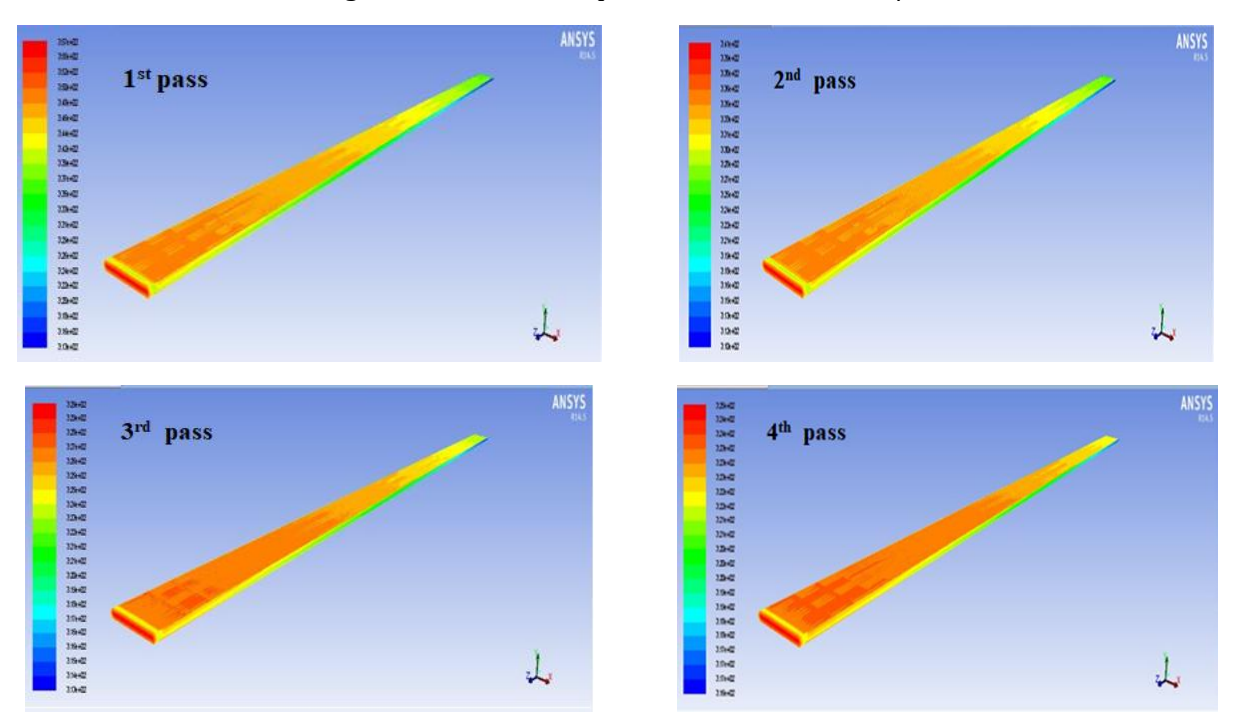
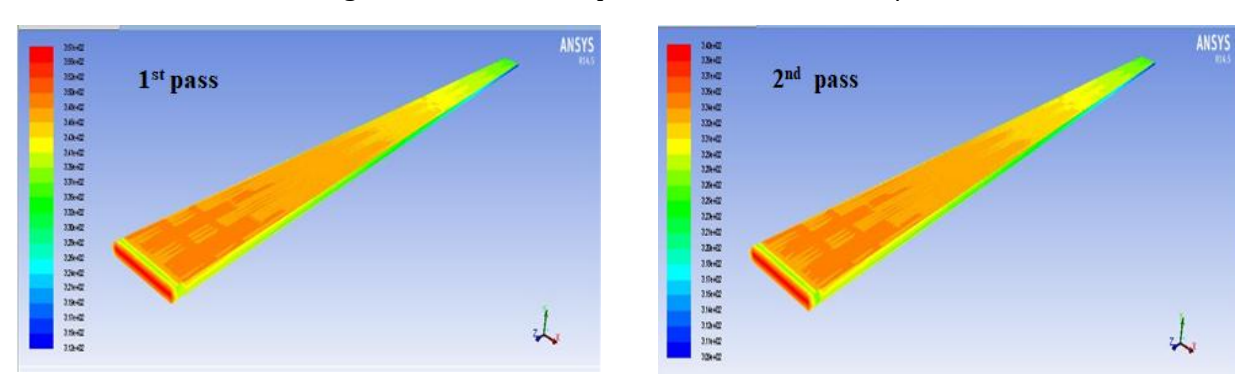


Fig. 20. Hexa tube temperature contour at 5 m/s



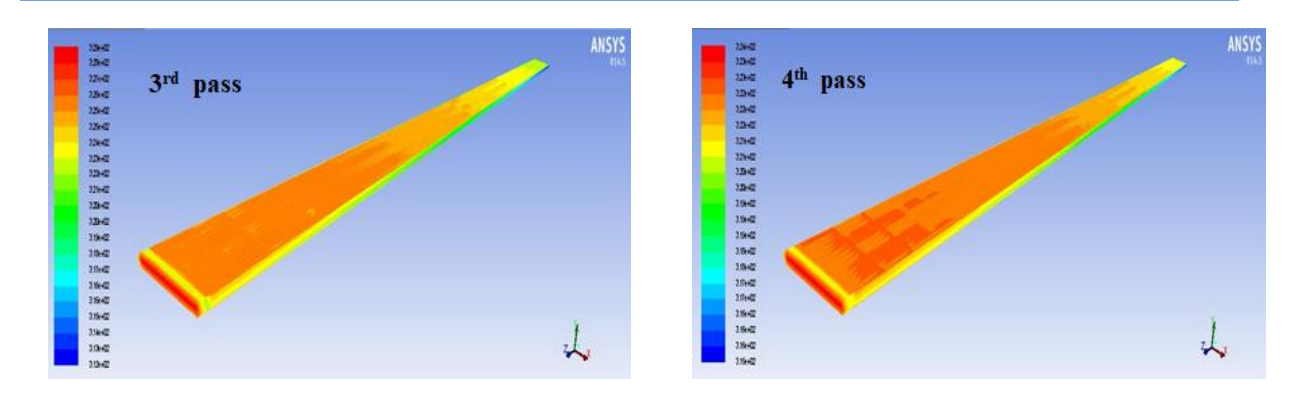


Fig. 21. Hexa tube temperature contour at 8 m/s

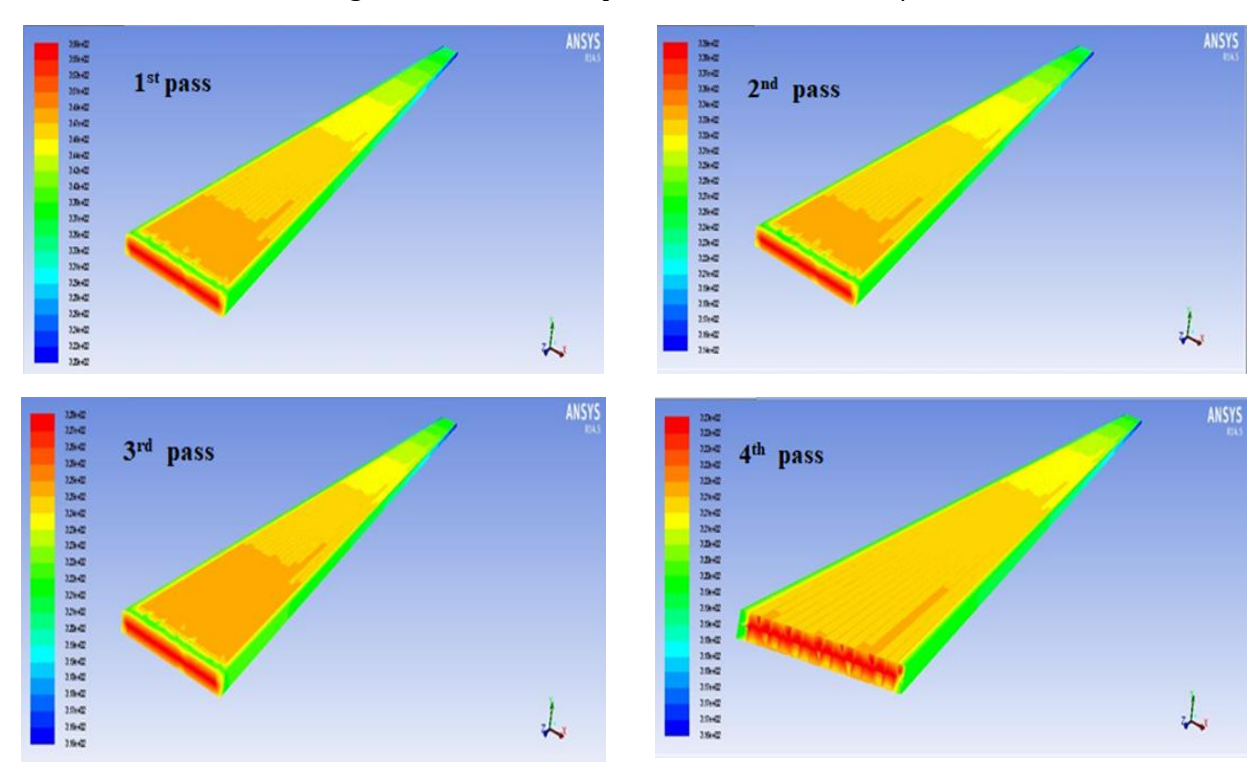
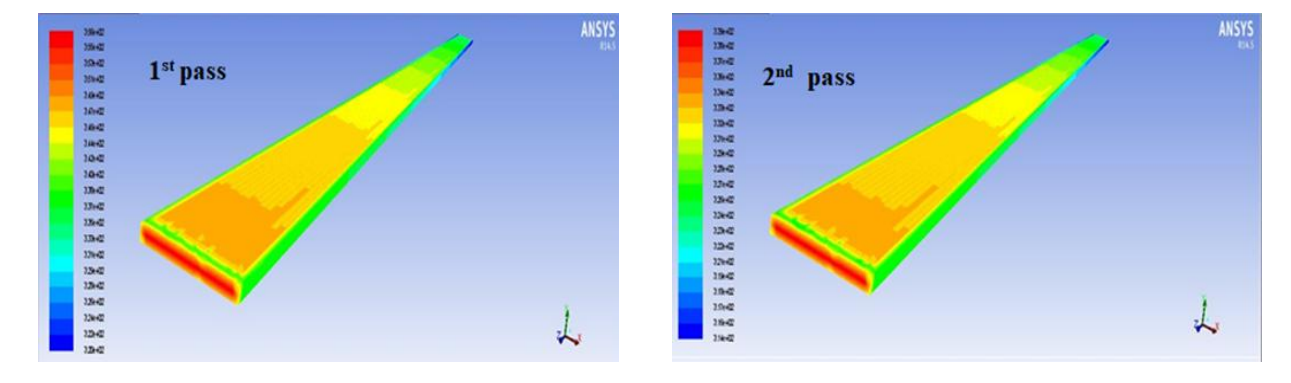


Fig. 22. Rectangular tube temperature contour at 2 m/s



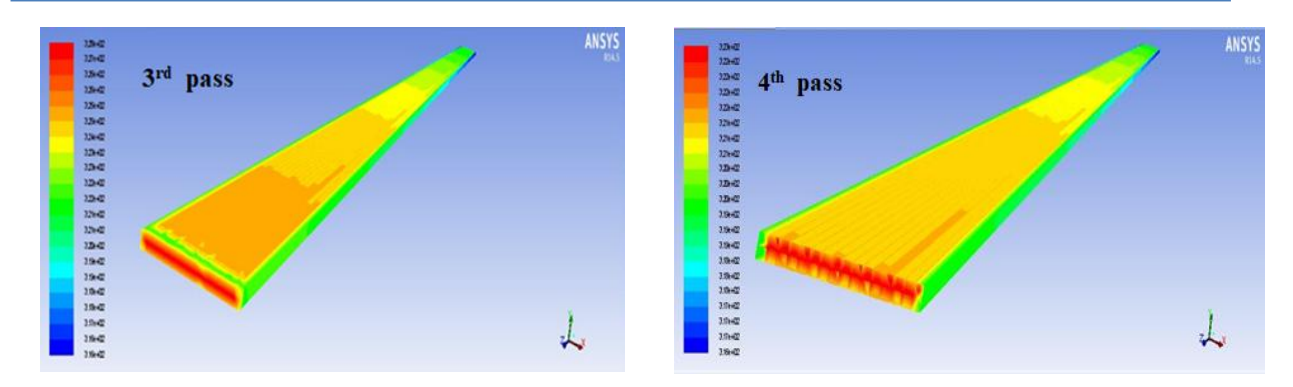


Fig. 23. Rectangular tube temperature contour at 5 m/s

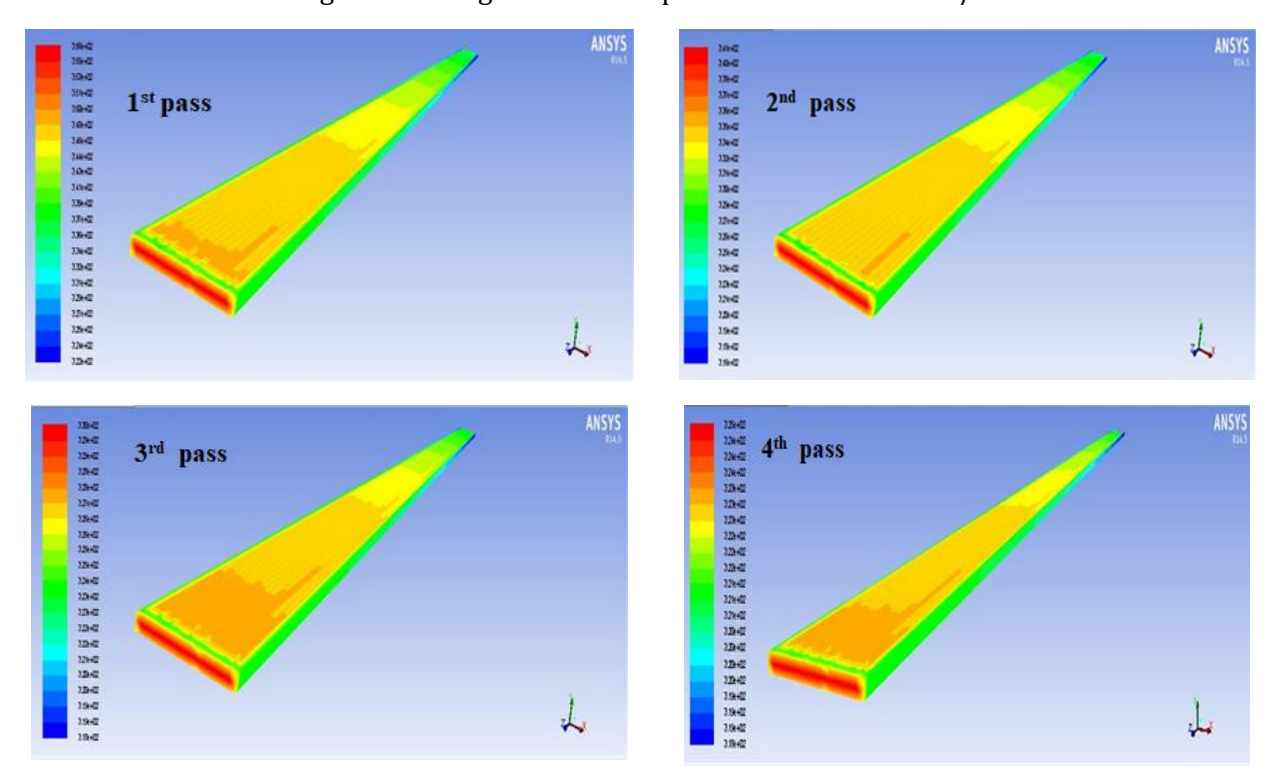


Fig. 24. Rectangular tube temperature contour at 8 m/s

Figures 14 and 15 show overall pressure and temperature distribution across the condenser for two-phase flow of refrigerant. The figures 16-24 show the CFD simulation being carried out for hexagon, oval, and rectangle shapes at the air velocities of 2 m/s, 5 m/s, and 8 m/s, respectively. The CFD simulation considered two-phase refrigerant flow for a 4-pass condenser configuration. This simulation helps to compare the results with the experimental & analytical study.

Table 9 presents the comparison of refrigerant outlet temperature based on CFD and analytical calculations. Table 10 summarizes the pressure drop from CFD and experiments. Numerical results were compared with experimental ones for pressure drop; it gives good agreement in the error percentage as shown in Table 10. Table 9 shows 5 to 16% variation in the outlet refrigerant temperature between CFD & experimental results. But Table 10 shows 3 to 10% variation in the pressure drop between CFD & experimental results. The result shows some acceptable error percentage between experimental and CFD results.

Table 9. Comparison of Refrigerant Outlet Temperature of CFD & Analytical calculation.

		Ova	al Tube P	rofile	Hexagonal Tube Profile			Rectangular Tube Profile		
			Refrigerant outlet Temperature in °C							
Air flow (m/s)	Pass	CFD analysis	Experimental	% deviation	CFD analysis	Experimental	% deviation	CFD analysis	Experimental	% deviation
	1	65	68.4	5.1	65.9	67.9	3.0	66.3	68.4	3.0
2	2	52.7	59.6	11.6	54	58.9	8.4	54.6	59.5	8.3
۷	3	48	56.3	14.8	48.7	55.6	12.4	49.8	56.2	11.5
	4	46	54.8	16.1	46.7	54.2	13.8	47.7	54.8	13.0
	1	66.7	69.5	4.0	67.4	69.0	2.3	67.9	69.4	2.2
_	2	55.2	60.7	9.1	56.3	60.0	6.2	57	60.6	5.9
5	3	50.7	57.3	11.6	51.6	56.6	8.9	52.4	57.3	8.5
	4	48.7	55.9	12.9	49.5	55.2	10.4	50.3	55.8	9.9
	1	66.1	68.6	3.7	66.8	68.2	2.1	67.4	68.6	1.7
8	2	54.3	57.6	5.7	55.4	57.3	3.3	56.3	57.6	2.2
Ö	3	49.7	52.4	5.3	50.7	52.3	3.2	51.6	52.4	1.6
	4	47.7	50.3	5.2	48.6	50.2	3.3	49.5	50.3	1.6

Table 10. Summary of pressure drop variation from CFD and Experiments

Ref. Mass flow rate	Outlet temp	Pressure drops (mbar)		
(Kg/s)	(°C)	Experimental	CFD	
0.054	44	708	730	
0.096	43.5	1842	1959	
0.113	43.5	2455	2674	

#### 7. Conclusion

The aim of this study is to improve condenser performance by incorporating unique tubes and shapes that control the volume of refrigerant. As per the aim, the study on different condenser tube shapes is made, and the summary of major findings is as follows:

- Of all the correlations, the refrigerant side Friedel correlation fits with experimental data the best, with differences of less than ±10%. Therefore, for analytical calculations for the varied tube geometries, Friedel correlation was employed.
- To comprehend the discrepancy between the CFD values and experimental ones of pressure loss and temperature across the tube, a CFD simulation was later run for various tube forms and ports.
- Further comparison of the CFD findings with the actual data revealed that, for various mass flow rates of the refrigerant, the variance ranged from 3 to 10%.
- Based on the extensive work done on the analytical calculation by using various correlations, it helped to understand the impact of variable tube geometry in the design phase of the product development in the automotive application.
- The rectangular model offers low heat transfer coefficient values in addition to low pressure drops.
- The hexagon model has a larger heat transfer coefficient and a higher pressure drop.
- Hexagon with rectangular port configuration is more suitable than other shapes such as rectangular & oval tubes.

Overall, the findings demonstrated that the analytical technique could be used in the first stage of product development in the automobile industry and that it could subsequently be connected with experimental data. This will shorten the lead time to market and avoid the expense of developing prototype parts. By lowering the size and effectiveness of the mobile air conditioner, a two-phase variable fin shape helps to increase the condenser's efficiency, which in turn lessens the total load on the compressor and, ultimately, increases the vehicle's fuel efficiency.

#### **Nomenclature**

```
- Mass flow
m
m_{\text{flux}}
                     - mass flux
           - Vapor quality
Х
                    - Liquid and Vapor density
\rho_{l} \& \rho_{g}
                    - Homogeneous density
ρн
D_h
                    - Hydraulic diameter
ReL&ReG - Reynold's number of liquid and Vapor
                    - Reynold's number of the film
F_{Lo\ \&}\ F_{Go}
                    - Friction factor of the liquid and Vapor
                    - Dynamic viscosity of liquid
ш
                    - Dynamic viscosity of vapor
\mu_g
           - Frictional pressure drop
Fr. We. E. F. H
                    - dimension less numbers
                     - multiplication factor for pressure drop
           - shear stress(wall)
\delta^+ and T_d^+
                    - Dimensionless parameter
Pr_L
                     - Prandel number
                    - Refrigerant side heat transfer coefficient in
h_{r}
                    - tube frontal flow area
A_f
```

#### References

- [1] Srisomba R, Asirvatham L, Mahian O, Dalkiliç A, Awad M, Wongwises S. Air-side performance of a microchannel heat exchanger in wet surace conditions. Thermal Science. 2017;21(1). https://doi.org/10.2298/TSCI150906227S
- [2] Sridhar K, Bicha K. Comparative Analysis of Parallel and Counter Flow Heat Exchangers. International Journal of Scientific Engineering and Technology Research. 2017 Feb;6(4):638-44.
- [3] Kabar Y, Rebay M, Kadja M, Padet C. Numerical Resolution of Conjugate Heat Transfer Problem in Parallelplate Micro-Channel. InCONV-09. Proceedings of International Symposium on Convective Heat and Mass Transfer in Sustainable Energy 2009. Begel House Inc. <a href="https://doi.org/10.1615/ICHMT.2009.CONV.280">https://doi.org/10.1615/ICHMT.2009.CONV.280</a>
- [4] Singh S, Kukreja R. Experimental heat transfer coefficient during condensation of R-410A in horizontal micro-fin tubes. InJournal of Physics: Conference Series 2019 Jul 1 (Vol. 1240, No. 1, p. 012052). IOP Publishing. <a href="https://doi.org/10.1088/1742-6596/1240/1/012052">https://doi.org/10.1088/1742-6596/1240/1/012052</a>
- [5] Achaichia A, Cowell TA. Heat transfer and pressure drop characteristics of flat tube and louvered plate fin surfaces. Experimental Thermal and Fluid Science. 1988 Apr 1;1(2):147-57. <a href="https://doi.org/10.1016/0894-1777(88)90032-5">https://doi.org/10.1016/0894-1777(88)90032-5</a>
- [6] Chang YJ, Wang CC. A generalized heat transfer correlation for Iouver fin geometry. International Journal of heat and mass transfer. 1997 Feb 1;40(3):533-44. <a href="https://doi.org/10.1016/0017-9310(96)00116-0">https://doi.org/10.1016/0017-9310(96)00116-0</a>
- [7] Kim MH, Bullard CW. Air-side thermal hydraulic performance of multi-louvered fin aluminum heat exchangers. International journal of refrigeration. 2002 May 1;25(3):390-400. https://doi.org/10.1016/S0140-7007(01)00025-1
- [8] Kim NH. Single-phase pressure drop and heat transfer measurements of turbulent flow inside helically dimpled tubes. Journal of Enhanced Heat Transfer. 2015;22(4). https://doi.org/10.1615/JEnhHeatTransf.2016016494

- [9] Liang YY, Liu CC, Li CZ, Chen JP. Experimental and simulation study on the air side thermal hydraulic performance of automotive heat exchangers. Applied Thermal Engineering. 2015 Aug 5;87:305-15. https://doi.org/10.1016/j.applthermaleng.2015.05.018
- [10] Wijayanta AT, Miyazaki T, Koyama S. Liquid-vapor phase distribution in horizontal headers with upward minichannel-branching conduits. Experimental Thermal and Fluid Science. 2016 Sep 1;76:264-74. <a href="https://doi.org/10.1016/j.expthermflusci.2016.03.021">https://doi.org/10.1016/j.expthermflusci.2016.03.021</a>
- [11] Panda K, Hirokawa T, Huang L. Design study of microchannel heat exchanger headers using experimentally validated multiphase flow CFD simulation. Applied Thermal Engineering. 2020 Sep 1;178:115585. <a href="https://doi.org/10.1016/j.applthermaleng.2020.115585">https://doi.org/10.1016/j.applthermaleng.2020.115585</a>
- [12] Jiang H, Aute V, Radermacher R. CoilDesigner: a general-purpose simulation and design tool for air-to-refrigerant heat exchangers. International Journal of Refrigeration. 2006 Jun 1;29(4):601-10. https://doi.org/10.1016/j.ijrefrig.2005.09.019
- [13] Yang L, Du X, Yang Y. Improvement of thermal performance for air-cooled condensers by using flow guiding device. Journal of Enhanced Heat Transfer. 2012;19(1). https://doi.org/10.1615/JEnhHeatTransf.2011002707
- [14] Lockhart, W. R. (1949). Proposed correlation of data for isothermal two-phase, two-component flow in pipes. Chemical engineering progress, 45(1), 39-48.
- [15] Friedel, L. (1979). Improved friction pressure drop correlations for horizontal and vertical two-phase pipe flow. In European two-phase group meeting, Ispra, Italy.
- [16] Chisholm, D. (1967). A theoretical basis for the Lockhart-Martinelli correlation for two-phase flow. International Journal of Heat and Mass Transfer, 10(12), 1767-1778. <a href="https://doi.org/10.1016/0017-9310(67)90047-6">https://doi.org/10.1016/0017-9310(67)90047-6</a>
- [17] LiangYe MW, Zeng X. Design and analysis of multi Parallel Pass Condensers'. International Journal of Refrigeration. 2009;32. <a href="https://doi.org/10.1016/j.ijrefrig.2009.01.012">https://doi.org/10.1016/j.ijrefrig.2009.01.012</a>
- [18] Liu Y, Sun W, Wu W, Wang S. Gas-liquid two-phase flow distribution in parallel micro-channels with different header and channels' orientations. International Journal of Heat and Mass Transfer. 2017 Sep 1;112:767-78. <a href="https://doi.org/10.1016/j.ijheatmasstransfer.2017.05.029">https://doi.org/10.1016/j.ijheatmasstransfer.2017.05.029</a>
- [19] Cavallini A, Del Col D, Doretti L, Matkovic M, Rossetto L, Zilio C. Two-phase frictional pressure gradient of R236ea, R134a and R410A inside multi-port mini-channels. Experimental Thermal and Fluid Science. 2005 Aug 1;29(7):861-70. https://doi.org/10.1016/j.expthermflusci.2005.03.012
- [20] Bensafi A, Borg S, Parent D. CYRANO: a computational model for the detailed design of plate-fin-and-tube heat exchangers using pure and mixed refrigerants. International Journal of Refrigeration. 1997 May 1;20(3):218-28. https://doi.org/10.1016/S0140-7007(96)00052-7
- [21] Valladares OG, Perez-Segarra CD, Rigola J. Numerical simulation of double pipe condensers and evaporators. International Journal of Refrigeration. 2004;27:656-70. <a href="https://doi.org/10.1016/j.ijrefrig.2004.01.006">https://doi.org/10.1016/j.ijrefrig.2004.01.006</a>